Washington University in St. Louis

Washington University Open Scholarship

Mechanical Engineering and Materials Science Independent Study

Mechanical Engineering & Materials Science

12-14-2017

Aerodynamic Study of Stability and Control of Straight Flying-Wings

Kevin Hainline
Washington University in St. Louis

Ramesh K. Agarwal
Washington University in St. Louis

Follow this and additional works at: https://openscholarship.wustl.edu/mems500

Recommended Citation

MEMS 500-09: Independent Study
Aerodynamic Study of Stability and Control of Straight Flying-Wings

Kevin Hainline
Advisor: Prof. Ramesh Agarwal

The bell-spanload, or bell-shaped lift distribution, gives proverse yaw for outer aileron deflections, a key factor in controlling a tailless vehicle. Study of bell-spanload applications have been limited to swept wings with elevon control schemes, relying on a well-tuned proverse yaw response for a differential elevon deflection. In examining unswept wings, symmetric outer control surface deflections have minimal associated pitching moment, allowing their use in adjusting the lift distribution to optimize for a wide range of flight conditions.

Lateral-directional control of bell-spanloads can be improved by the use of an additional set of ailerons inboard of the mid-span vortices. The inboard ailerons provide traditional adverse yaw which serves as a linearly independent control vector relative to the existing proverse yaw outer surfaces; the two vectors are sufficient to define a parallelogram-shaped controllable region in the roll-yaw control space.

Nomenclature

CL   =   Lift Coefficient for a Wing

c   =   Chord

b   =   Span

Λ =   Sweep Angle

L   =   Lift

L' =   Lift per Unit Span, or "Sectional Lift"

L'_0 =   Sectional Lift of the Root Chord

MAC   =   Mean Aerodynamic Chord

IWCS   =   Inboard Wing Control Surface

OWCS   =   Outboard Wing Control Surface

UAV   =   Unmanned Aerial Vehicle

I. Introduction

A. Optimal Spanloads

For a constant lift and a constant span, the elliptical lift distribution is optimal for minimizing induced drag:

$$L' = L_0' \left(1 - \left(\frac{y}{b/2}\right)^2\right)^{1/2} \tag{1}$$

If the span constraint is removed and the root-bending-moment kept constant, then the bell-spanload is optimal for minimizing induced drag. This was identified by Prandtl in 1933[1], as well as separately by R.T.Jones at NACA:[2]

$$L' = L_0' \left(1 - \left(\frac{y}{b/2}\right)^2\right)^{3/2} \tag{2}$$

Taking into account viscous drag or higher fidelity parametric estimates for wing weight will result in optimal spanloads which lie somewhere between the elliptical and bell-shaped spanloads, as shown by Klein and others[3][4][5][6][7]. There are as many "optimal" spanloads as there are ways to constrain wing geometry, but the main focus of this paper is on a side-effect of the bell-spanload: proverse yaw.

The bell-spanload has the unique property of trailing vortices shedding at a point mid-span rather than the traditional "wing-tip" vortices. This mid-span point is at approximately 70% of the half-span and occurs at the inflection point in the lift distribution[8]. The region outboard of the mid-span vortex is of significance since partial induced-drag recovery is acheived here in the form of "induced-thrust". Since the Lift Vector is tilted forward in this region, control deflections which increase lift also increase induced thrust locally. As a result, yaw due to roll is proverse.

B. Recreating the Prandtl-D Glider

The advantages of the bell-spanload in tailless stability and control were demonstrated at the Armstrong Flight Research Center under the guidance of Al Bowers. His team developed the "Prandtl-D" tailless glider which was stable and controllable using only direct elevon control by a line-of-sight radio-control pilot.[8] Using the geometry defined in his paper, "On Wings of the Minimum Induced Drag: Spanload Implications for Aircraft and Birds", I was able to recreate the Prandtl-D Glider in XFLR5, a vortex-lattice analysis tool.
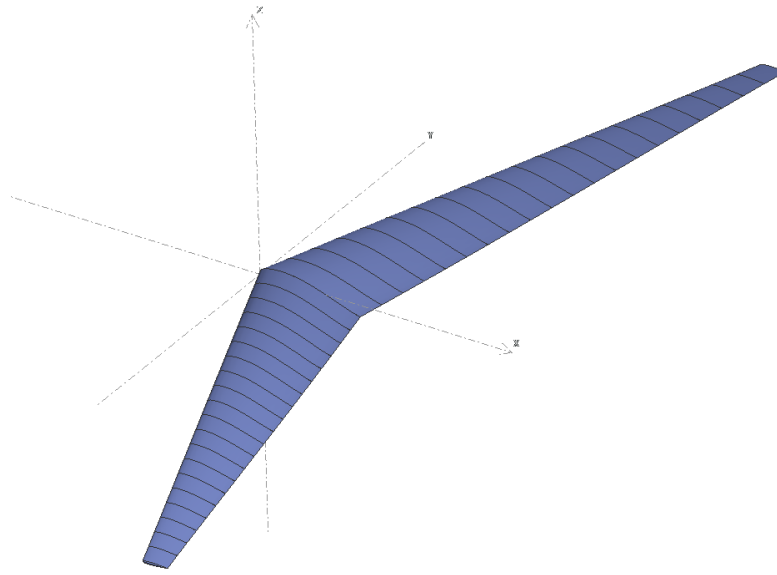
Fig. 1   Isometric View of Prandtl-D XFLR5 Model

Operating at a CL of 0.62, the results I generated differed from the published results some, particularly near the root. The root airfoil specified in the Bowers paper was neither normalized (trailing edge ending at x=1.00) nor de-rotated (trailing edge ending at y=0) leading to some ambiguity on how chord and twist are specified. The analysis was conducted for the airfoils as-is and also normalized and de-rotated. The figures below show the normalized and de-rotated results which were slightly improved, but still did not completely satisfy the bell-spanload. Nonetheless, the general behavior was still demonstrated (see Fig. 2), including the all-important negative induced drag at the wingtips (see Fig. 3).
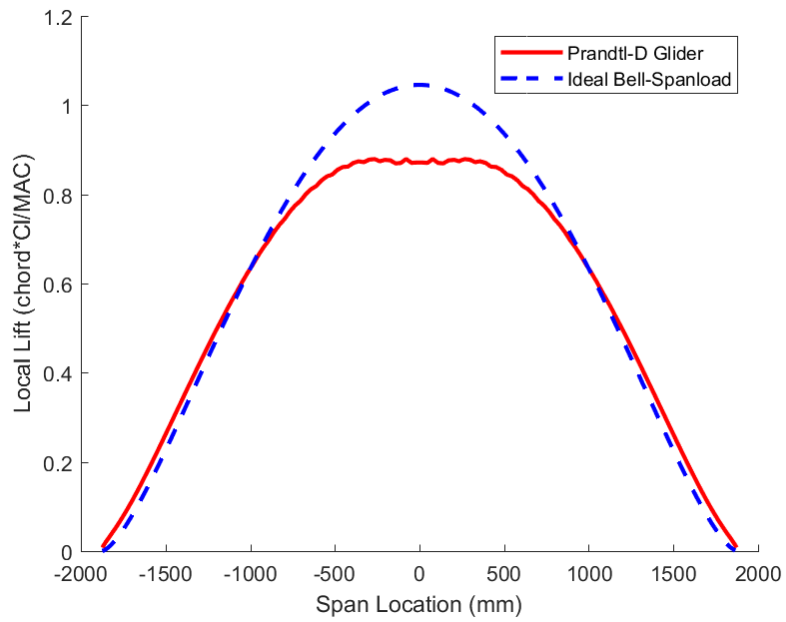
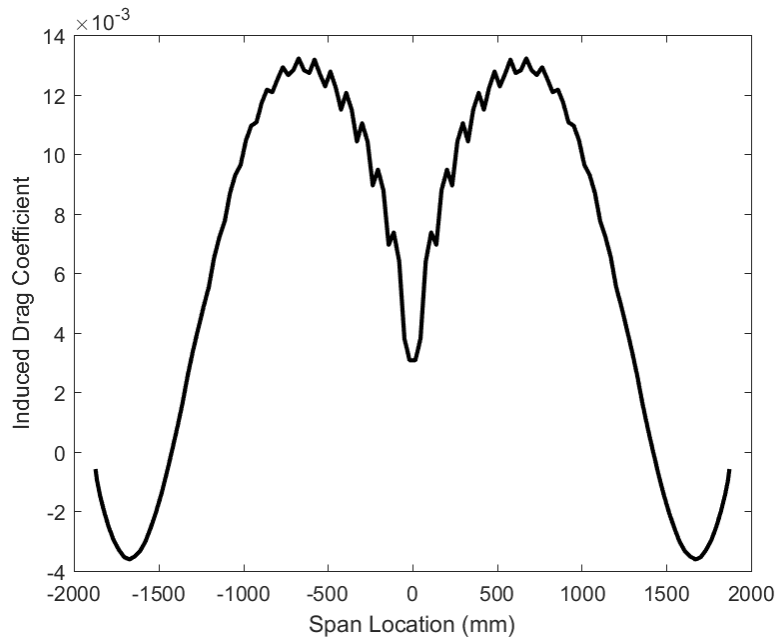**Fig. 2   Lift Distribution Comparison to Ideal for the Prandtl-D Glider**

Fig. 3   Induced Drag Distribution of the Prandtl-D Glider

II. The Straight Flying Wing

A. Concept

As seen in the prandtl-D glider, existing configurations of flying-wing bell-spanloads have been swept-back. Bringing the wing straight offers certain advantages, the most obvious one being a performance increase. If the bell-spanload is the minimum induced drag (under certain constraints), then using it in a context of a swept-wing for non-transonic applications counteracts the benefit that is to be gained from the bell-spanload. To a first order approximation, efficiency is proportional to $cos(\Lambda)$, meaning a 20-degree sweep (as in the Prandtl-d) results in roughly a 6% hit to aerodynamic efficiency. The impact to equilibrium and control is more subtle: the prandtl-D glider uses a complex twist-scheme, specified at 21 different span locations. This particular twist was optimized to produce the bell-spanload for a specific trim condition. Whether by differing payloads or flying conditions, a versatile platform is expected to operate effectively at different overall lift coefficients. For a swept wing, these are acheived by shifting the trim angle of attack using elevon deflections. Thus, not only does the bell-spanload degrade when operating at the non-design-point CL (with no way to correct it without adversely affecting trim), the elevon deflections necessary to fight static stabilty further degrade the lift-distribution, particularly at the wing-tips, the critical location for drag-recovery.

On a straight wing, control surface deflections have managable pitching moments. Particularly, in a linear sense, all-moving ailerons which rotate about the quarter-chord have no pitching moment. This allows the twist to be varied to optimize the lift distribution at each flight condition. Also, conveniently, this all-moving outer aileron maximizes the bell-spanload proverse yaw effect.[9] For the moment, all-moving outer control surfaces have not been analyzed, this will be the subject of future research.

Analyzing the straight-wing bell-spanload is the next step in understanding avian flight. If proverse yaw is the solution for lateral-directional control, it should be applied in the same manner in an unswept wing with a short body-flap at the root for pitch-control. Longitudinally, the straight-flying-wing is a horrendous conglomeration of undesirable flight dynamics characteristics, and likely the reason why it hasn't yet been pursued.

- Issues include:
  - low control power
    * airfoil pitching moments can't be trimmed out, so reflex is necessary
    * only very small static margins are trimmable
  - very low aerodynamic pitch damping
  - very low pitch inertia

Such vehicle characteristics necessitate tight closed-loop control in order to improve the longitudinal flying qualities and yet this vehicle shape is found in birds. Thus a biomimetic discrete flight controller is taking on the role of a bird's "balance" or "piloting". Henceforth the straight-flying-wing with bell-spanload and root-body elevator will be referred

to as the biomimetic blended-wing-body or biomimetic bwb.

The root-body elevator, in this case, is analagous to a bird's tail. Note that it is expected that birds also use small changes in sweep for pitch control, directly manipulating the center of lift and thus the pitching moment. However, the effectiveness of this method is proportional to the operating lift coefficient and thus cannot fully explain bird flight at during all flight phases (i.e. in a dive). In any case, the manipulation of sweep for pitch control is not easily transferrable to artifical flying vehicles due to the high demands on the sweep actuators (fighting a large moment of inertia) and the heavy hinges required (must carry all of the lift). Variable wing sweep as a primary flight control is outside of this study's scope.

B. The Biomimetic Blended-Wing-Body UAV

In order to study the viability of a straight-wing bell-spanload configuration, I examined the handling qualities of a 4kg, 2 meter wing-span biomimetic BWB UAV:
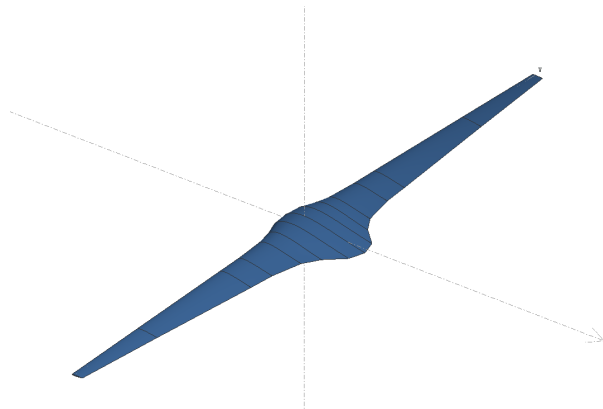

Fig. 4   Isometric View of the Biomimetic BWB XFLR Model

The outer three-quarters of the span is straight-tapered and can be easily constructed using only two "panels" of foam cut with a hot wire. That is, the geometry is fully defined by lofting between only 3 airfoils. The inner quarter of the span is a more complex spline which increases the root chord, this is intended to be constructed out of balsa allowing for internal space for electronics. All airfoils are EH tailless airfoils and those with camber also have reflex. The root has the greatest camber and thickness, and this lofts down to the tip which is thin and symmetrical. The quarter-chord line is precisely along the body y-axis. That is, no quarter-chord sweep or dihedral. The exact camber, thickness, twist, and chord are defined in Table 1.

Table 1   Wing Geometry Definition

y(mm)	chord (mm)	twist(deg)	camber(%)	thickness (%)
0	270.0	6.0	3.0	15
50	250.0	5.5	3.0	15
100	180.0	5.0	3.0	15
150	140.0	6.25	2.5	10
250	113.8	6.75	1.5	9
333	105.0	7.0	1.0	9
704	66.1	3.75	0.0	9
1000	35.0	-1.0	0.0	9

Having a larger root chord has many advantages in the biomimetic configuration. Larger chord results in a greater moment arm for the elevator, which is a plain flap located around the root chord. larger chord also results in greater total thickness for a constant airfoil percent-thickness. Large total thickness at the root is useful for storing flight batteries, avionics, and general payload. In order to maintain the bell spanload at cruise the root section must be de-twisted some (about 3 degrees twist originally), resulting in a lower local lift coefficient. As a result, this portion of the wing will stall last, allowing good pitch control to be maintained through a stall. Lift coefficient and other spanwise distributions are shown below:
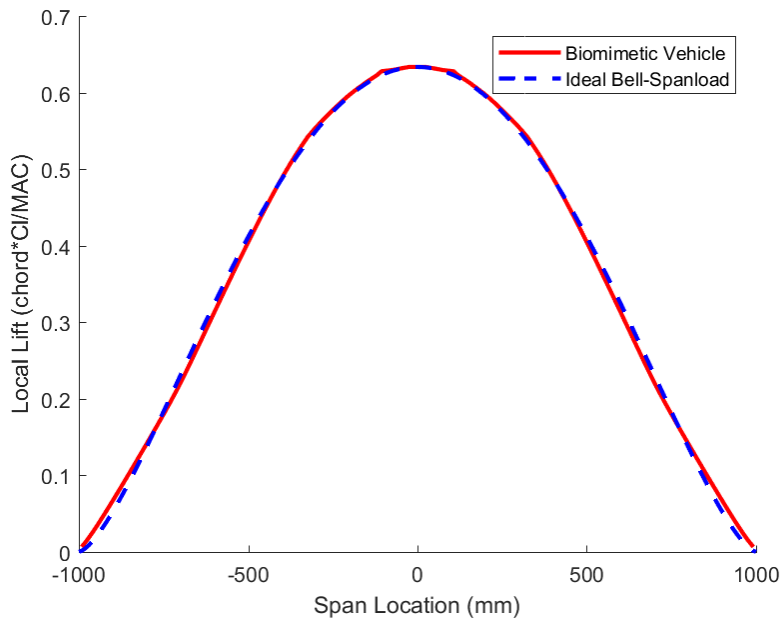

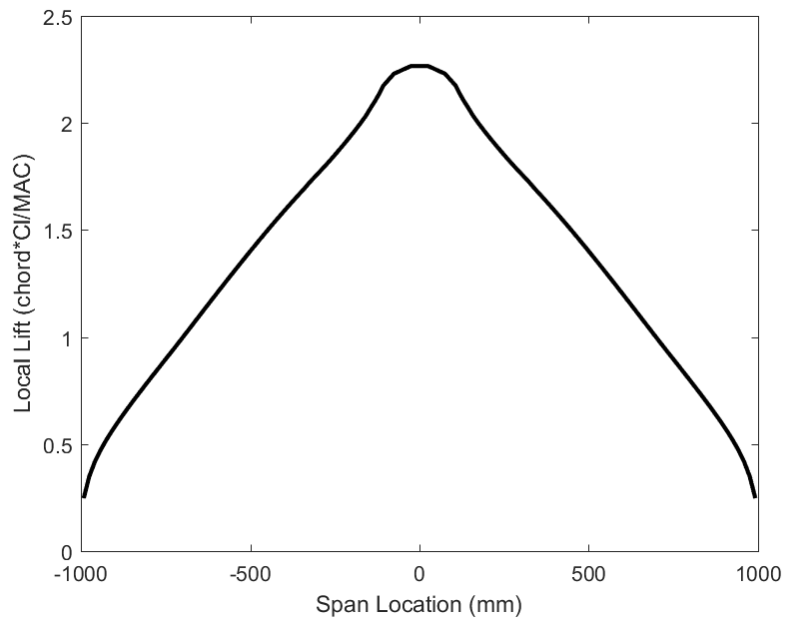**Fig. 5   Lift Distribution Comparison Against Ideal**
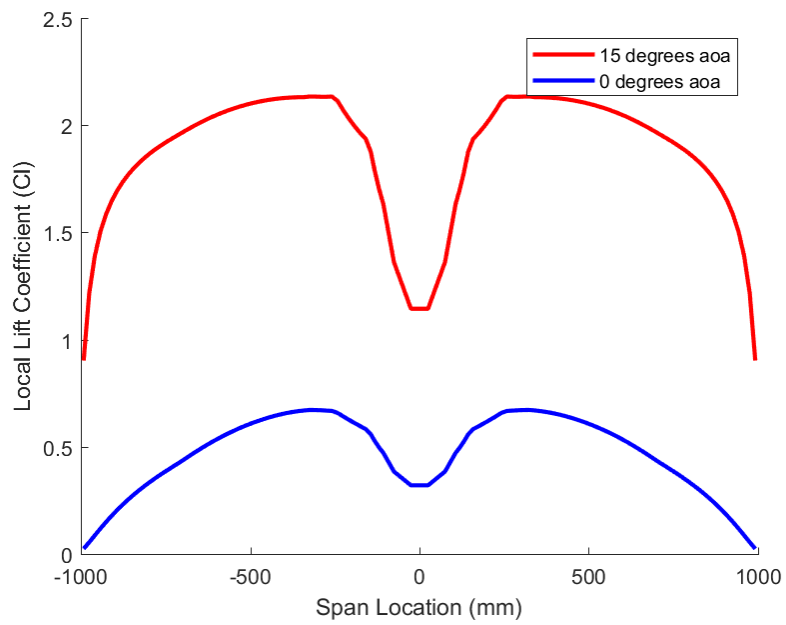
Fig. 6   Lift Distribution Near Stall

Fig. 7   Lift Coefficient Distribution at Cruise and Near Stall
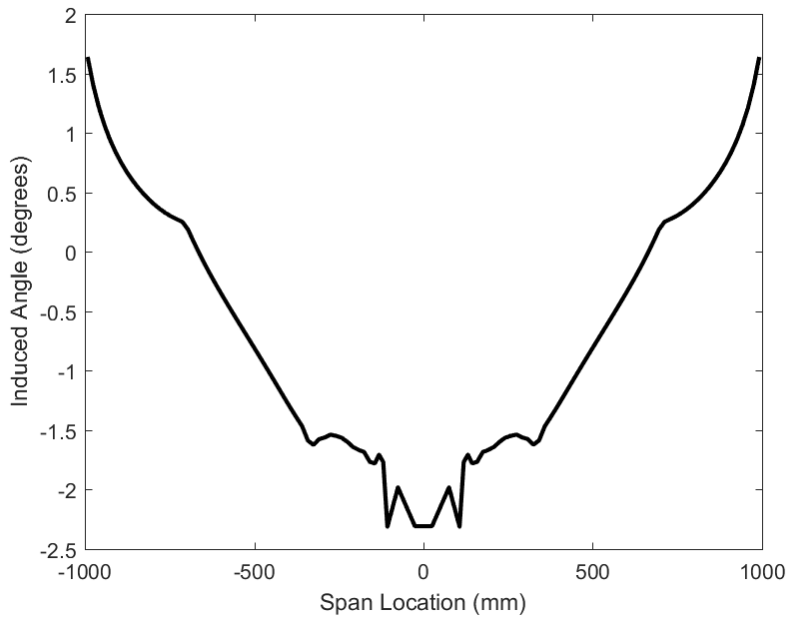
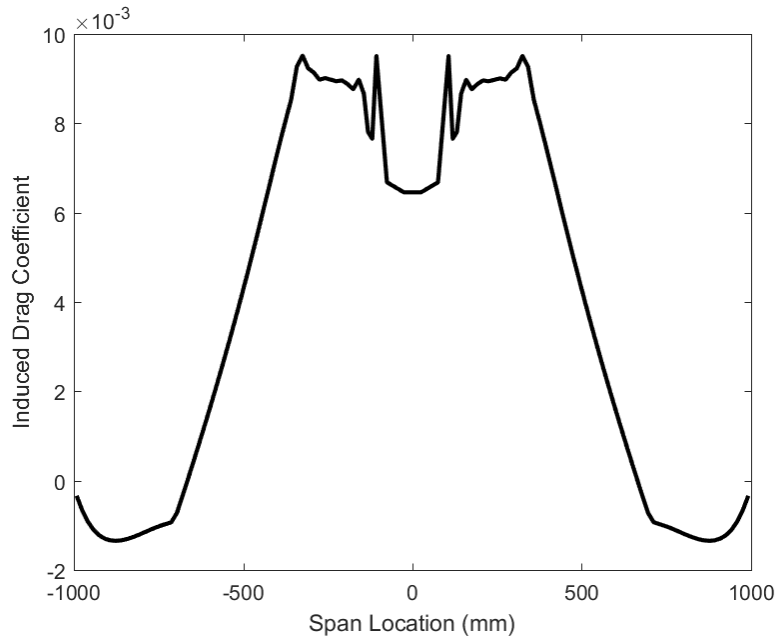**Fig. 8   Induced Angle Span Distribution at Cruise**

Fig. 9   Induced Drag Span Distribution at Cruise

Three degrees of pitch-up elevator deflection were necessary to trim the vehicle, this was incorporated into the base airfoil shape of the inner two wing sections. The twist profile was tuned to match the ideal bell spanload, as shown in Fig. 5, this meant that although the inner sections were originally heavily de-twisted, their elevator deflections meant bringing the twist back up, resulting in the final twist distribution shown in Table 1. The distortion of the planform area

9

near the root has advantages in stall behavior, as seen in Fig. 7, but also distorts the induced drag coefficient distribution near the root, as seen in Fig 9. This design still shows induced thrust on the outboard portion of the wing, as well as low total induced drag.

III. Stability and Control Analysis

While XFLR5 was useful for quick design iterations in developing the geometry, it lacks key capabilities for analyzing the effect of control surfaces. Namely, the induced drag distribution caused by asymmetric control deflections cannot be accessed or exported, only the total moments are outputs of the program for asymmetric wings. As a result, the biomimetic configuration was also modelled in OpenVSP, another vortex-lattice software which has more options for control surface configuration and analysis.

A. Stability - Linear Plant Characteristics

Longitudinally, both modes are poorly damped, as expected. However, these modes are stable and the ratio of control power to stability is high meaning the longitudinal plant characteristics allow for closed-loop stabilization.
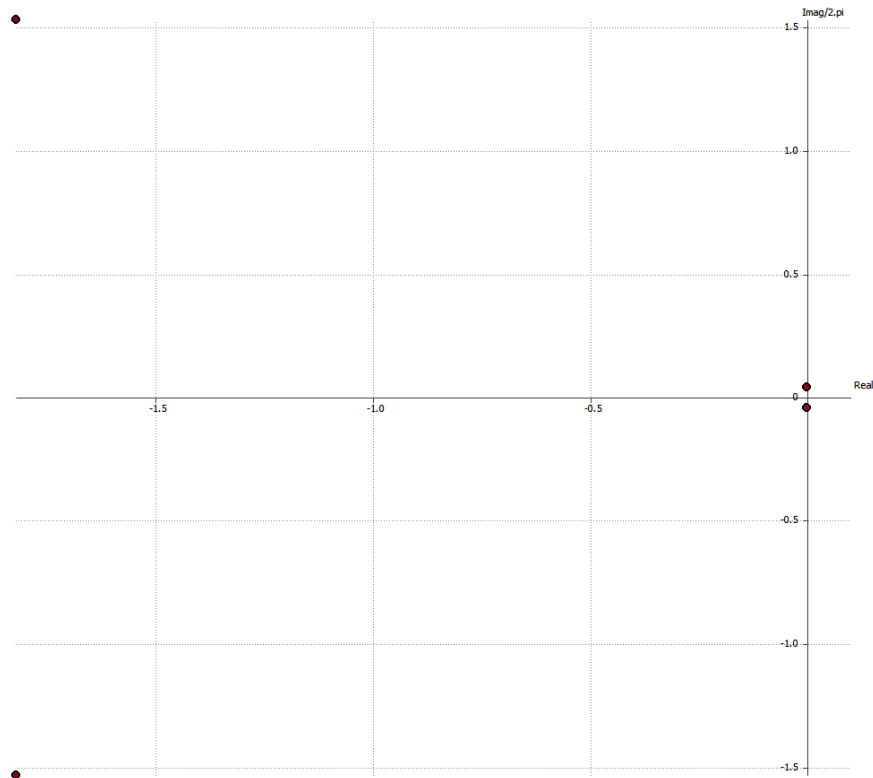

Fig. 10   Longitudinal Pole/Zero Plot

Lateral Directional eigenvalues also look poor but managable. The spiral mode time to double is high, dutch roll is horribly damped but stable, and roll subsidence is great. There are two issues with this plant behavior when designing a

flight controller around it. Firstly, the yaw control power may be insufficient, and secondly, with such low sideforce generated, an observer will have trouble estimating sideslip. As long as proverse yaw can be replicated, control power should be sufficient, though the observer issue has no readily apparent solution and direct measurement of sideslip may be required. The simplest solution would be a sideslip vane, but this adds a vertical surface which would ruin an otherwise vertical-surface-less vehicle (perhaps the primary motivation for such a vehicle in the first place). A 5-hole probe or similar air-data system is likely needed for this configuration.
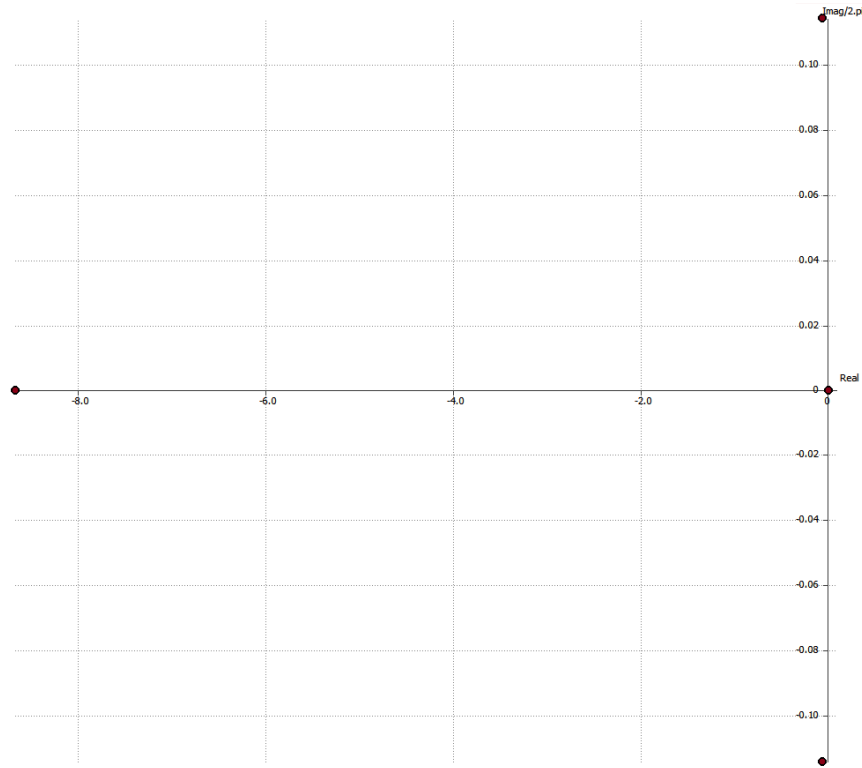

Fig. 11   Lateral-Directional Pole/Zero Plot

B. Control

The elevator span fraction is 0.1 and the chord fraction is 0.2, the elevator is located at the root and once constructed may need to be split up into two separate elevators to accomodate the trailing-edge curvature (and provide redundancy). In this application, longitudinal control does degrade the lift distribution, so in future iterations even neutral stability is preferred such that control deflections are not necessary to maintain trim. Cruise at all flight conditions would be acheivable with no steady state deflections, only small corrective transients.

Table 2   Longitudinal Control Derivatives

	$X_{\delta e}$	$Z_{\delta e}$	$M_{\delta e}$
Elevator	0.18	7.0	353

11

The biomimetic configuration does acheive proverse yaw using outer ailerons, albeit barely, and not entirely in the manner expected. Rather than a larger magnitude of induced thrust on the "lifting" side pulling the rising wingtip forward, the dominating source of proverse yaw is from less induced thrust on the "spoiled" side, letting the falling wingtip also slide backward. Since proverse yaw is acheived through manipulation of the existing lift distribution, it is expected that the magnitude and perhaps the behavior itself is dependent on the wing loading. That is, higher design lift-coefficients have greater induced angles which creates more robust induced thrust in the outer-span regions; this creates a favorable environment for proverse yaw even under large control deflections. Additionally, higher wing-loadings are advantageous for dynamic soaring flight[10], which is one application of this configuration in nature (the wandering albatross) as well as a possible application for future aircraft (high-altitude long-endurance UAVs). This, and other proverse-yaw optimization techniques will be the subject of future research.

Control power was determined from small (2 degree) deflections, acting as a finite difference approximation for linear control power near the neutral position. Though each set of control surfaces produces a strong rolling moment, it is not suitable to call these surfaces ailerons since they accomplish other flight control functions (yaw, lift-distribution manipulation, and even pitch). Rather, they are indentified on a more simple level: Inboard Wing Control Surface (IWCS) and Outboard Wing Control Surface (OWCS). The IWCS starts at $\frac{y}{b/2} = 0.5$ and ends at $\frac{y}{b/2} = 0.7$ using a chord fraction of 0.25. The OWCS starts at $\frac{y}{b/2} = 0.76$ and ends at $\frac{y}{b/2} = 0.855$ using a chord fraction of 0.35.
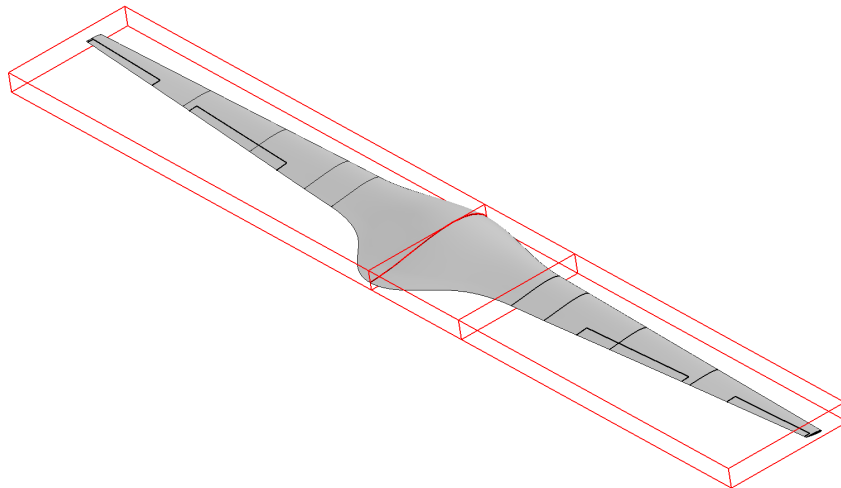

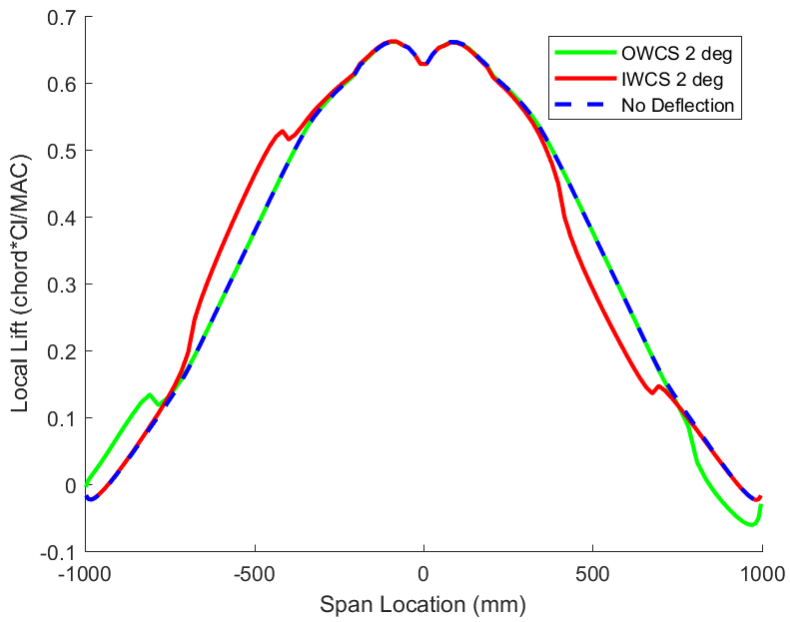**Fig. 12   Isometric View of Biomimetic BWB Model with Control Surfaces in OpenVSP**

Fig. 13   Lift Distribution in OpenVSP With Different Control Deflections
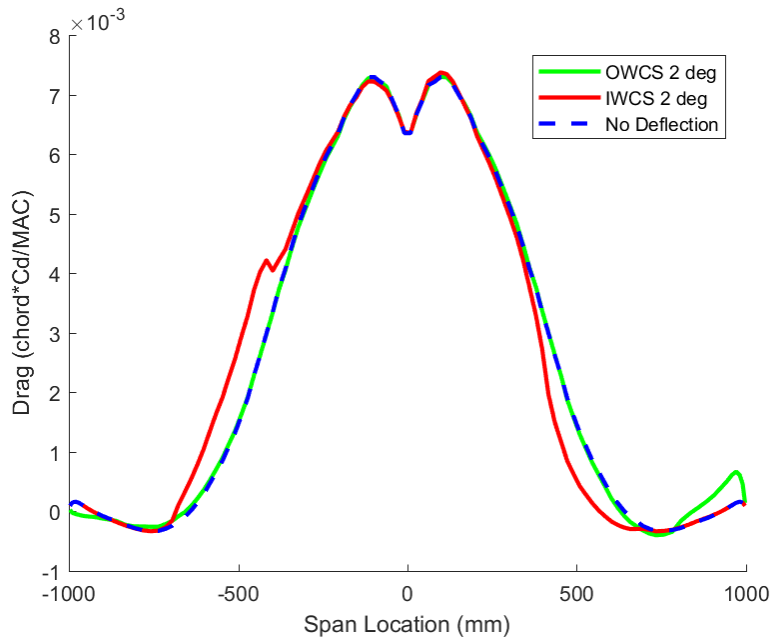

Fig. 14   Drag Distribution in OpenVSP With Different Control Deflections

The lateral-directional control derivatives are listed below

Table 3   Lateral-Directional Control Derivatives

Surface	$C_l \delta a$	$C_n \delta a$
OWCS	0.0013	3.34e-06
IWCS	0.0019	-1.87e-05

Using both sets of control surfaces, a flight controller for this vehicle would have a parallelogram-shaped region of control in the roll-yaw control plane:
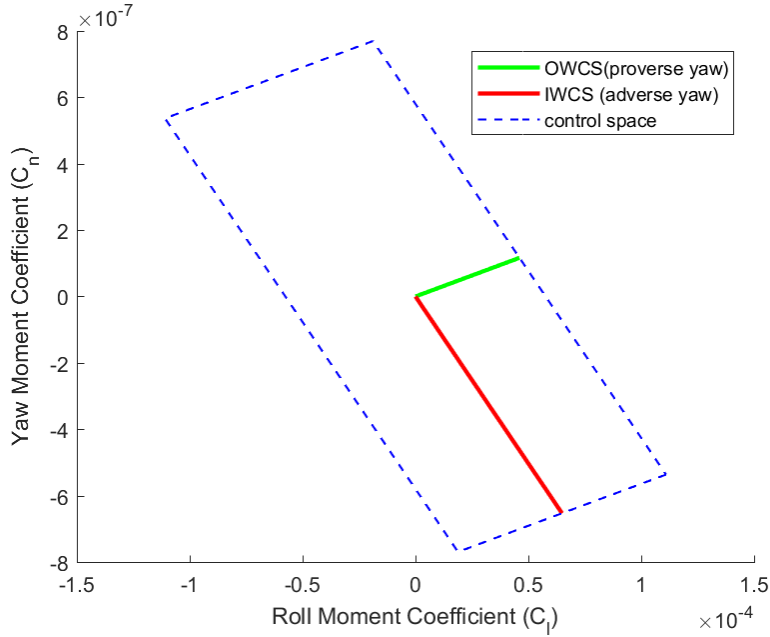

Fig. 15   Lateral-Directional Control Space

C. Non-Linear Validation

A finite area of lateral-directional control space is expected to improve robustness and command-tracking performance compared to only having a single vector to work with (one set of control surfaces, as in Prandtl-D). A high-fidelity non-linear vehicle model has been created in order to compare control schemes such as these, and validate flight controller designs.

Actuators are modeled as second-order with hysteresis and including their control linkages, propulsion is modelled using the UIUC propeller database for the propeller and linear motor characteristics for the brushless-DC motor (i.e.: K_v and K_T). Multi-dimensional table lookups are used to allow for a non-linear aero database, and the flight controller itself is integrated with this vehicle model as a discrete system operating in runtime conditions.
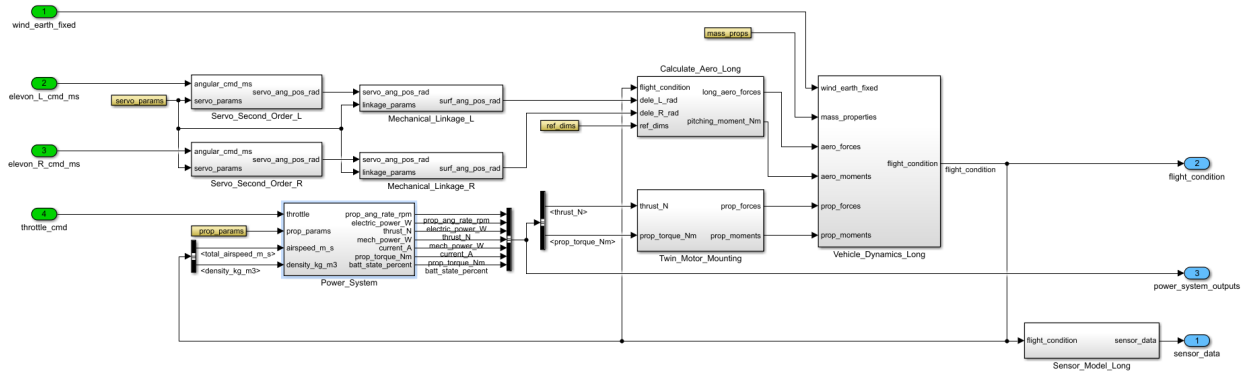
Fig. 16   High-Fidelity Simulation: Vehicle Model Top Level

This simulation environment will have three operating modes: longitudinal, lateral-directional, and full six-degree-of-freedom. This is a key element of future research in order to demonstrate the controllability and closed-loop stability of straight-flying-wings.

IV. Conclusions

Optimizing proverse yaw imposes a different set of requirements on the geometry of the vehicle, simply using a bell-spanload is insufficient to guarantee strong proverse-yaw characteristics. On the same vehicle proverse yaw and adverse yaw can be achieved using control surfaces in different locations relative to the mid-span vortex, verifying that arbitrary roll-yaw combinations are possible within a parallelogram-shaped control space. The straight-flying-wing is fully controllable without relying on thrust vectoring and could have application where high performance and robustness is required for small payload volumes.

Acknowledgments

References

[1] Prandtl, L., "On Wings with Minimum Induced Drag," *Zeitschrift Flugtechnik und Motorluftschiffahrt*, Vol. 24, 1933.

[2] R.T.Jones, "The Spanwise Distribution of Lift for Minimum Induced Drag of Wings Having a Given Lift and a Given Bending Moment," *NASA Tech Note No. 2249*, 1950.

[3] Klein, A., and Viswanathan, S., "Approximate Solution for Minimum induced Drag of Wings with a Given Structural Weight," *AIAA Journal of Aircraft*, Vol. 12, No. 2, 1975.

[4] Wroblewski, G., "Prediction and Experimental Evaluation of Planar Wing Spanloads for Minimum Drag," *University of Illinois at Urbana-Champaign Thesis Paper*, 2016.

[5] Iglesias, S., and Mason, W. H., "Optimum Spanloads Incorporating Wing Structural Weight," *AIAA, Aircraft, Technology Integration, and Operations Forum*, AIAA, Los Angeles,CA,USA, 2001. doi:10.2514/6.2001-5234.

[6] *The Minimum Induced Drag of Aerofoils*, NACA Report No. 121, 1923.

[7] *A Method for Determining the Camber and Twist of a Surface to Support a Given Distribution of Lift, with Applications to the Load Over a Sweptback Wing*, NACA Report No. 826, 1945.

[8] Bowers, A. H., and Murillo, O. J., "On Wings of the Minimum Induced Drag: Spanload Implications for Aircraft and Birds," *NASA/TP-2016-219072*, 2016.

[9] Kuhlman, B. . B., "On The Wing, Twist Distributions for Swept Wings," *R/C Soaring Digest*, Vol. 20, No. 6, 2003, p. 6.

[10] Barnes, J., "How Flies the Albatross, The Flight Mechanics of Dynamic Soaring," *SAE International*, 2004. doi:10.4271/2004-01-3088.